Time-Average Velocity and Turbulence Measurement Using Wireless Bend Sensors in an Open Channel with a Rough Bed

Robert L. Stewart, S.M.ASCE[1]; James F. Fox, M.ASCE[2]; and Cindy K. Harnett[3]

Abstract: This paper is motivated by the need to develop low cost, wireless velocity sensors for hydraulic research and application in streams. A velocity bend sensor (VBS) is a flexible plastic polyimide substrate sheet with an electronic resistor connected to a voltage divider. Drag of a moving fluid bends the sensor, changes the electronic resistance, and produces a voltage drop that can be related to the time-averaged freestream velocity of the fluid. VBSs were tested in a recirculating hydraulic flume with a gravel bed. The VBSs show transition from rigid to elastic bending with increasing freestream velocity, which can be described using dimensionless fluid and beam-bending properties. The relationship between stream velocity and voltage drop across the circuit is nonlinear. A semitheoretical approach to estimate time-averaged streamwise velocity from the voltage drop based on fluid drag, elastic member bending, and circuit principles is applied and shows good agreement with experimentally derived calibration curves. The triple decomposition theorem and spectral analysis are performed on VBS and acoustic Doppler velocimeter (ADV) time series. Results show that the VBS captures low-frequency characteristics of macroturblence present within the turbulent open channel flow but is unable to measure smaller-scale characteristics of eddy shedding for these hydraulic conditions. Turbulent intensity calculated using VBS data is 12% of that from the ADV attributed to the lack of detection of shedding-sized eddies. But, the linear fit between turbulent intensity from the VBS and ADV suggests that the VBS can be used as a proxy for more detailed turbulent measurements when applied in streams. **DOI: 10.1061/(ASCE)HY.1943-7900.0000725.** © *2013 American Society of Civil Engineers.*

CE Database subject headings: Probe instruments; Decomposition; Spectral analysis; Turbulence; Open channels; Velocity; Flow measurement.

Author keywords: Sensor network; Macroturbulence; Decomposition; Spectral analysis; Turbulent intensity.

Introduction

The present research is motivated by the need to develop low cost, wireless velocity sensors for hydraulic measurements within highly sensed stream monitoring networks. Emphasis was placed upon velocity sensor measurements of time-averaged velocity and turbulence in hydraulically rough open channel flow with a gravel bed, which are typical hydraulic conditions in streams. It is recognized that inexpensive sensors and sensor networks show promise for stream measurements such as mean velocity and turbulence parameters. Inexpensive sensor networks could potentially assist with measuring the mean velocity spatially in a cross section for stage-discharge relationships, which would decrease the need for manually collected measurements under dangerous flooding conditions. Inexpensive, wireless sensors also show promise for measuring the mean flow and turbulence in pools and transition zones in streams in order that aquatic biologists can link hydraulic diversity with fish habitat conditions and functioning (Hauer and Lamberti 2006). Further, spatially distributed sensors will be useful for verifying the hypothesized double layer of turbulence in streams, which includes connected vortex packets that eject from the bed, and macroturbulence in the outer region (Duncan 1970; Adrian et al. 2000; Roy et al. 2004; Hurther et al. 2007; Fox and Belcher 2011) as well as measure large three-dimensional eddies induced by channel bathymetry and large obstructions (Kwan 1988; Fox et al. 2005; Nezu 2005). Finally, as computational fluid dynamics modeling becomes more sophisticated and applied, sensor network measurements of the flow field could be used to calibrate model parameters (Maier et al. 2010).

The existing need for inexpensive hydraulic sensors is met by recent advancement in electronics and sensing. Recent technological developments in the miniaturization of electronics and wireless communication have begun a revolution in environmental sensor networks (Hart and Martinez 2006; Yick et al. 2008; Rundel et al. 2009). Recent advancement in sensor network technology promotes inexpensive measurements of environmental parameters in space and time so that fluxes operating at the process scale can be integrated to the large scale (Hart and Martinez 2006; Horsburgh et al. 2010). New sensor technologies are focusing on wireless due to low cost, small size, low power requirements, and faster installation (Wang et al. 2006). Wireless sensors offer researchers the ability to monitor remote or dangerous environments where many processes have rarely been studied due to their inaccessibility (Hart and Martinez 2006). Field measurements with automated mobile wireless velocity sensors combined with georeferencing

[1]Graduate Associate, Civil Engineering Dept., Univ. of Kentucky, Lexington, KY 40506.

[2]Associate Professor, Civil Engineering Dept., Univ. of Kentucky, Lexington, KY 40506 (corresponding author). E-mail: jffox@engr.uky.edu

[3]Associate Professor, Electrical Engineering Dept., Univ. of Louisville, Louisville, KY 40292.

Note. This manuscript was submitted on March 12, 2012; approved on December 19, 2012; published online on December 21, 2012. Discussion period open until December 1, 2013; separate discussions must be submitted for individual papers. This paper is part of the ***Journal of Hydraulic Engineering***, Vol. 139, No. 7, July 1, 2013. © ASCE, ISSN 0733-9429/2013/7-696-706/$25.00.

technology have the possibility to reduce errors and time delays associated with manual monitoring techniques (Vivoni and Camilli 2003).

Although it appears the need for inexpensive hydraulic sensors is fulfilled with new sensor network technology, very few studies have reported detailed investigations of applicable sensors. Mechanical meters such as the propeller meter have been widely used for some time, but angular momentum of the propeller affects their ability to measure turbulence within sensor networks (Rehmel 2007). For velocity and turbulence measurements in shallow streams, the predominant instruments used are the acoustic Doppler velocimeter (ADV) and electromagnetic current meter (ECM) (Buffin-Belanger and Roy 2005). The ADV and ECM provide accurate measurements of velocity and turbulence but are relatively expensive for use within sensor networks. Mobile transmission technology is revolutionizing the way in which water velocity measurements are being transferred from the field; however, many of these measurements are still being obtained manually (Vivoni and Camilli 2003). Inexpensive, wireless, low power velocity sensors are needed that offers the possibility of taking measurements at temporal and spatial scales necessary for highly sensed stream-monitoring networks.

The objective of this research is to present, investigate, and verify inexpensive wireless velocity sensors for hydraulic measurements. The newly developed velocity sensors are called velocity bend sensors (VBS) (Harnett et al. 2011). This paper provides a detailed study of VBSs and their ability to measure time-averaged velocity and turbulence characteristics of open channel flow with a rough bed typical of stream conditions where the VBS can be implemented. This paper provides: (1) A full description of the VBS mechanical, electrical, and wireless transmission characteristics are presented. Fabrication of the VBS from commercially available components is also described. (2) An experimental method to calibrate and verify the VBS for use in open channel flow with a rough bed is described. (3) Experimentally derived calibration curves are presented for the VBS that relate time-averaged stream velocity to sensor voltage, and the behavior of the sensor in bending is related to dimensionless fluid and bending properties. A semi-theoretical approach based on fluid drag and elastic member bending is used to continuously estimate time-averaged stream velocity using VBS measurements. (4) The ability of the VBS to measure prominent turbulent scales and turbulence intensity of open channel flow over a rough bed is examined through the use of eddy decomposition via the triple decomposition theorem, spectral analysis, and turbulence statistics.

Velocity Bend Sensors

The newly developed wireless sensors are called velocity bend sensors due to their operating mechanism [see Fig. 1(a)]. Water velocity causes the sensor, which acts as a strain gage, to bend and change the electrical resistance of the sensor [Fig. (1b)]. The basic circuit of the VBS is depicted in Fig. 1(a) and consists of a voltage divider. A fixed (10 kΩ) resistor is placed in series with a variable resister (e.g., Flexpoint brand bend sensor) and is powered by a 5 V power source (Harnett et al. 2011). The bend sensor has a base resistance of approximately 4 kΩ and increases up to 30 kΩ when deflected. The voltage drop across the bend sensor is measured and used as the calibration voltage. The VBS can be interfaced with an onboard A/D chip (e.g., the Maxim DS2450), which converts the analog voltage read to a digital format. Wireless communication with the VBS is made possible using a wireless sensor node (e.g., the Crossbow Technology TelosB), which is connected to the onboard A/D chip using the 1-wire protocol. Data can be collected on a PC or data storage hub from approximately 30 m away using a second node.

Fabrication of the VBS can be performed by purchasing commercially available parts from home improvement stores and an electronics supplier. Assembling the electronic components requires some basic knowledge of circuits and the capability to solder. The housing for electronic components is constructed from polyvinyl chloride to prevent the electronics from contacting water and provides a means to deploy the sensors in the stream. The 4-AA battery pack and the wireless node are housed in the top of the polyvinyl chloride housing, which is above the free surface. Wires connect the sensors to the wireless node and are contained within the polyvinyl chloride housing. A more detailed description of the construction of the VBS can be found at http://salamandersensors.org/.

The VBS are designed to be deployed across a stream network to meet the needs of researchers for high temporal and spatial data resolution. The VBS have a low hardware cost of approximately $20 per sensor. The low cost of the VBS allows deployment in large

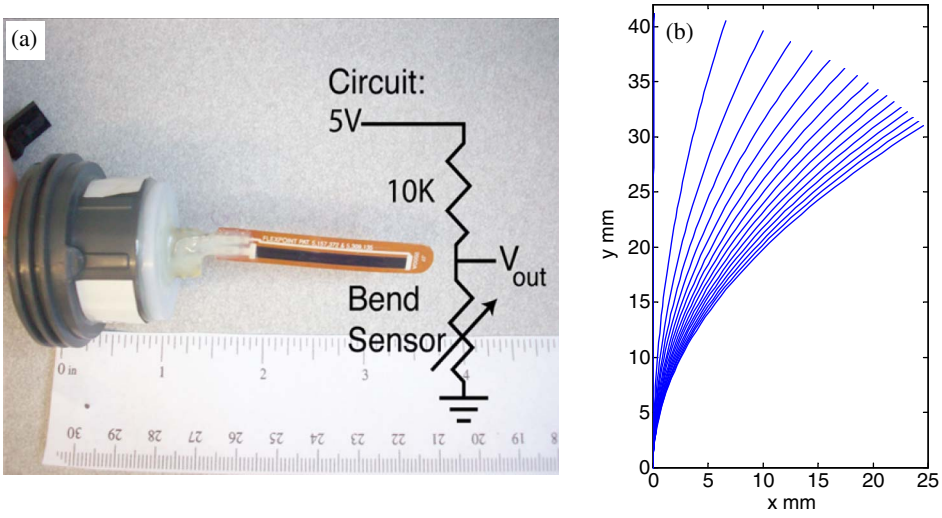

Fig. 1. (a) Photograph of a VBS with a depiction of electronic behavior; (b) approximate deflected shape of the VBS in bending when increasing from 0 to 80 cm s^{-1} in 5 cm s^{-1} increments

J. Hydraul. Eng. 2013.139:696-706.

numbers and reduces the cost associated with lost or damaged sensors. The VBS were designed using components that have a small power demand, which allows VBS deployment for reasonable amounts of time using a self-contained battery power supply. The VBS battery life is a function of power demand per location and the frequency at which data are collected, but for reference a VBS that samples once every 2 min can operate for at least a week in the field. The wireless communication capabilities provided by the wireless node enables multiple VBSs to send data to a localized data storage unit, which makes data retrieval from a stream network time-efficient (Harnett et al. 2011). The wireless signal can also be relayed to a long-range communication device so that researchers can view data without ever physically going to the field. The quasi-real-time data provided by the wireless capabilities of the VBS allow researchers to remotely quality check the health of the sensor network.

Experimental Method

The experimental method was designed to test (1) time-averaged velocity and (2) turbulence measurement capabilities of the VBS. A range of mean streamwise velocity conditions typical of a stream was sought after. To represent a wide range of conditions, two experimental apparatuses were used during testing, including a water tunnel and a hydraulic flume. A total of 18 tests were performed. In Table 1, the test apparatus and hydraulic conditions are indicated. Tests 1–9 were low flow conditions, and testing was performed in a water tunnel. Tests 10–14 were for the intermediate flow case and were performed in a zero gradient hydraulic flume. Tests 15–18 were the highest stream velocity conditions and were performed in the hydraulic flume with the bed slope equal to 0.006 m m^{-1}. In Table 1, S = the bed gradient of the flume; H = the average flow depth; F = the Froude number [$\mathsf{F} = U_{\text{bulk}}(gH)^{-0.5}$, where U_{bulk} = the bulk velocity and g = gravity]; U_* = the shear or friction velocity; R = the channel Reynolds number ($\mathsf{R} = U_{\text{bulk}}H\nu^{-1}$, where ν = kinematic viscosity of the fluid); and k_s^+ = the roughness Reynolds number ($k_s^+ = k_s U_* \nu^{-1}$, where k_s = the bed roughness height). All tests were used to assess time-averaged VBS output and its ability to measure the time-averaged approach velocity, U. Tests 10–18 in the hydraulic flume were used for assessing the turbulent flow characteristics of the VBS. These tests represent hydraulically rough, low relative submergence of bed particles and moderate Froude number conditions, which are turbulent flow conditions typical of a stream.

Table 1. Hydraulic Conditions for Experimental Tests

Test number	Test apparatus[a]	S (m m^{-1})	U (cm s^{-1})	H (cm)	F	U_* (cm s^{-1})	R ($\times 10^4$)	k_s^+
1	WT	0	1.6	6	0.01	0.1	0.1	—
2	WT	0	6.0	6	0.05	0.4	0.4	—
3	WT	0	11.9	6	0.10	0.7	0.7	—
4	WT	0	17.7	6	0.14	1.1	1.1	—
5	WT	0	23.6	6	0.19	1.4	1.4	—
6	WT	0	26.5	6	0.22	1.5	1.5	—
7	WT	0	29.4	6	0.24	1.6	1.8	—
8	WT	0	32.4	6	0.26	1.8	1.9	—
9	WT	0	35.3	6	0.29	1.9	2.1	—
10	HF	0	25.6	7.9	0.28	1.9	2.1	109
11	HF	0	32.7	9.8	0.33	2.5[b]	3.2	139
12	HF	0	35.9	10.7	0.36	2.7	3.9	154
13	HF	0	43.3	12.6	0.40	3.2	5.6	182
14	HF	0	47.9	14.0	0.43	3.6	7.1	201
15	HF	0.006	61.1	8.5	0.64	4.6	5.0	258
16	HF	0.006	65.5	9.8	0.66	5.0	6.4	278
17	HF	0.006	69.6	11.4	0.68	5.3	8.3	298
18	HF	0.006	73.0	14.0	0.68	5.7	11.2	318

[a]WT = water tunnel; HF = hydraulic flume.
[b]Interpolated value since calibrated ADV incomplete, and thus results of this test are not included in Fig. 6.

For the relatively low flow Tests 1–9, a low-speed flow visualization water tunnel was used. The water tunnel was a Model 501-6" low-speed flow visualization water tunnel manufactured by Engineering Laboratory Design, Inc. The water tunnel is a closed circuit unit with a free water surface test section. The test section is 15.2 cm wide by 15.2 cm high by 45.7 cm long and constructed of type SAR, clear, acrylic, which allows for observation of the VBS during testing. Flow conditioning upstream of the test section is provided by a perforated cylinder to distribute the flow followed by stainless steel perforated plates that act as head loss baffles. The settling length, upstream of the contraction to the test section, is fitted with a tubular cell plastic honeycomb section. Three 60% porosity, stainless steel screens are mounted upstream of the test section. A twin turning vane cascades in the return direct flow leaving the test section. Flow velocity is variable in increments of approximately 0.6 cm s^{-1} from 0–35 cm s^{-1}. The maximum deviation in measured approach velocities to the VBS (±4%) was used as uncertainty bounds on the estimated water tunnel velocities.

To obtain the intermediate and high range velocities and test the turbulence measuring capabilities of the VBS in Tests 10–18, a 12 m long by 0.61 m wide closed circuit hydraulic flume with a fixed bed roughness (i.e., d_{84} equal to 5.6 mm) was used (Belcher and Fox 2009; Belcher and Fox 2011; Fox and Belcher 2011). Tests were performed 9 m downstream of the headbox and 3 m upstream of the flume outfall. Rods were placed at the outfall of the flume to reduce the hydraulic slope and force quasi-uniform flow in the test section. Approach velocities for the intermediate tests ranged from approximately 25 to 50 cm s^{-1}, which provided some overlap with the velocities tested for the low velocity tests. Approach velocities for the high flow tests ranged from 59 to 72 cm s^{-1}.

During testing, the VBS were placed on a 2.1 cm polyvinyl chloride mounting device with the same connections that would be used in the field. The mounting device was fastened to the top of the flume using a clamp and also stabilized at the bed to prevent flow-induced vibrations. After mounting the VBS, its elevation above the bed was measured. In the hydraulic flume, the elevation was referenced to halfway between the troughs and crests of the roughness elements to the centerline of the VBS. The data acquisition rate of the VBS is variable up to 200 Hz and was set at 50 Hz during testing. Flow stabilization was confirmed in both apparatuses prior to data collection. The output from the VBS was the voltage drop that occurs across the bent resistor in the voltage divider circuit and has units of volts. The voltages reported here are relative to a zero velocity voltage (V_0), which is the voltage reading taken when the sensor is unbent in stagnant conditions.

During the highest flow hydraulic flume Tests 15–18 (i.e., $S = 0.006$ m m^{-1}), the VBS mounting device produced a gradually varied flow upstream of the VBS. For these four tests, the time-averaged approach velocity at the VBS bending element was estimated using a modified log wake law for gradually varied flow and verified using velocity profiles measured upstream of the VBS. The modified log wake law was used to model the time-averaged streamwise velocity profile in decelerating hydraulically rough open channel flow where the shear velocity (U_*) and Cole's wake strength (Π) were adjusted for flow nonuniformity (Song and Graf 1994; Song and Chiew 2001; Onitsuka et al. 2009). The modified log wake law is given as

J. Hydraul. Eng. 2013.139:696-706.

$$\frac{U}{U_*} = \frac{1}{k}\ln\left(\frac{y}{k_s}\right) + B + \frac{2\Pi}{k}\sin^2\left(\frac{y\pi}{2H}\right) \quad (1)$$

where κ = the von Karman constant taken to be 0.4; k_s = the roughness height taken equal to d_{84}, which was 5.6 mm; B = the constant of integration for rough bed flows 8.5; and H = the flow depth. The value of U_* was found using turbulence measurements with an acoustic Doppler velocimeter and the Clauser method (Kirkgoz 1989; Nezu and Nakagawa 1993), which were in close agreement. Π is a function of the pressure gradient parameter, β (Song and Graf 1994; Onitsuka et al. 2009), which is given as

$$\beta = \frac{H}{\tau_0} g\rho\left(-S + \frac{dH}{dx}\right) \quad (2)$$

where τ_0 = the bed shear stress; and dH/dx = the hydraulic gradient. The value of Π is described as a function of β (Nezu et al. 1994; Song and Graf 1994; Onitsuka et al. 2009) given as

$$\Pi = 0.07\beta + 0.27 \quad (3)$$

The value of dH/dx in Eq. (2) was both measured and modeled in the analysis. The value of dH/dx was modeled using the St. Venant equation as

$$\frac{dH}{dx} = \frac{S - \frac{U_*^2}{gH}}{(1 - \mathrm{F}^2)} \quad (4)$$

The estimates for U were verified using measured velocity profiles with an ADV at (10, 15, 40, and 90 cm) upstream of the VBS. The RMS error was 2.1 cm s^{-1} for data collected within the sampling volume of the VBS providing uncertainty bounds for this method. The sampling volume for estimate of the approach velocity U was the same as that of the VBS (4 mm in the y-direction), and U was estimated by integrating across the modified log-wake law for this location.

In order to assess turbulence measurement of the VBS, its results were compared with ADV results. The ADV used for comparison was a SonTek acoustic Doppler velocimeter (16 MHz), which has a sampling rate of 50 Hz, velocity resolution of 0.01 cm s^{-1}, and accuracy of 1% of the measured velocity. The ADV has a small sampling volume approximately 0.1 cc that is located 5 cm from the transmitting transducer. The ADV was mounted on a rigid rod that was attached to the top of the flume and stabilized by the flume bed to avoid flow-induced vibrations; such vibrations may cause elevated intensity readings (Dancey 1990). The ADV was positioned 2 cm upstream of the VBS so that any flapping of the bend sensor did not affect the ADV signal. The 2 cm streamwise difference in locations was justifiable to assume as the same location with regards to measuring turbulence characteristics of the flow in the streamwise u-direction because (1) the vertical location of the sensors above the bed was the same, (2) the flow depth did not change over the 2 cm streamwise distance, (3) flow was hydraulically rough ($k^+ > 70$), (4) flow did not have pronounced secondary velocities at this location, and (5) flow was well above the roughness region at $y = 6d_{84}$. The authors have extensively studied the structure of turbulence and its imprint on the mean velocity in this flume for these hydraulic conditions, and at this vertical y-location the turbulent structure advects with the streamwise velocity rather than being connected to the bed (Belcher and Fox 2009; Fox and Belcher 2011; Belcher and Fox 2011). In postprocessing of the ADV data, the authors found that the velocity data sets were statistically stationary, which was verified using the first, second, third, and fourth statistical moments of velocity. Spectral analysis of the velocity data using 4,800 ADV measurements was performed. The ADV power spectral density exhibited a region with a $-5/3$ slope (in log-log scale) that shows the inertial subrange (see Fig. 2) (e.g., Singh et al. 2010).

Results of Time-Averaged Velocity

The general relationship between VBS shape and velocity is shown in Fig. 1(b); as velocity increases the VBS bends and the tip becomes more aligned with the flow. The greatest amount of curvature for the deflected shapes occurs near the connection location. Fig. 3 provides the time-averaged approach velocity versus output voltage for the tests shown in Table 1. Voltage output from the VBS in Fig. 3 is shown to be nonlinear due to the nonlinear bending response to velocity and the nonlinear relationship between resistance and radius of curvature. A transition velocity is shown to exist at around 35 cm s^{-1} in Fig. 3. Below the transition, deflections are small due to the large storage of elastic potential energy within the VBS as compared to the kinetic energy of the flow. The region above the transition is characterized by fluid kinetic energy that is larger than the elastic potential energy of the VBS. Large deflections result, and the shape becomes asymptotically quasi-parabolic.

A semitheoretical approach was used to relate the measured VBS voltage to the time-averaged approach velocity.

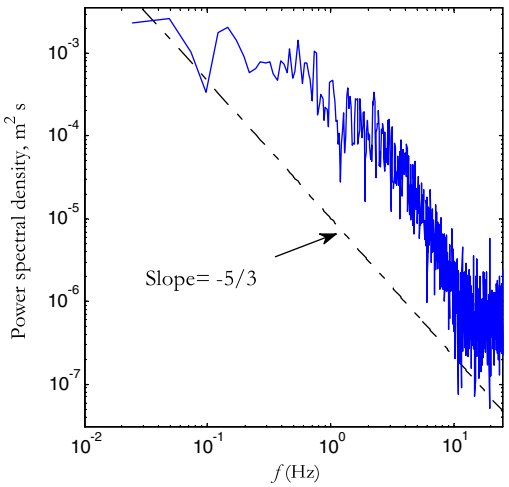

Fig. 2. Power spectral density of the ADV data

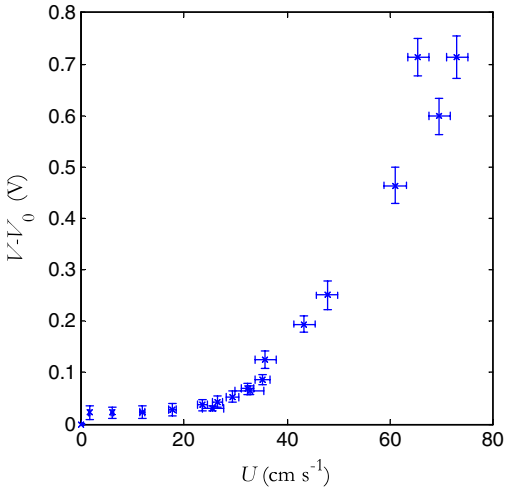

Fig. 3. Time-averaged approach velocity versus output voltage

J. Hydraul. Eng. 2013.139:696-706.

The semitheoretical approach logically follows from the fact that the fluid approach velocity deflects the VBS and causes its shape to be curvilinear due to fluid drag on the elastic member [see Fig. 1(b)]. In turn, the deflected shape increases electrical resistance in the member and increases the net voltage difference across the divider. Prediction of the deflected shape follows the fundamental work by Alben et al. (2002, 2004). Harnett et al. (2011) applied the fundamental work to bend sensors and provided the relationships between the deflected shape and electrical resistance. The approach introduced here builds off the earlier work and provides a calibration method for the VBS. In addition, the past methods were improved by changing the spatial scale used for the VBS, adding a parameter to account for turbulent flow conditions, modifying the equation used for element radius of curvature, and calibrating the predicted bent shape of the VBS using experimental photographs.

During bending by the approach fluid, the VBS is connected at one end and behaves as a cantilever beam. The shape of the member can be quantified using the dimensionless freestream speed, η (Alben et al. 2002, 2004). η is the ratio of fluid kinetic energy to the elastic potential energy of the member and can be formulated for the VBS as

$$\eta = C_t\sqrt{\frac{4\rho w L^3 U^2}{EI}} \tag{5}$$

where C_t = a turbulence coefficient; ρ (1 g/cm^3) is the fluid density; L and w = the length and width, respectively; E = the modulus of elasticity; and I = the beam moment of inertia. In principle, η describes the fluid forces versus elastic forces in the beam and was derived using potential flow theory. The bending theory accounts for the fact that the projected area of the bend sensor changes with velocity magnitude (Alben et al. 2002, 2004), and the turbulent coefficient can be used to adjust experimental data in hydraulically rough flow. Alben et al. (2004) found that shape self-similarity emerges when the bending element actual coordinates are properly scaled to η. Using η, the shape of the VBS scaled coordinates can be described by

$$Y = 1.34X^{1/2} \tag{6}$$

where the scaled coordinates (X and Y) are the actual coordinates (x and y) scaled by $\eta^{2/3}$ as

$$X = x\eta^{2/3} \tag{7a}$$

and

$$Y = y\eta^{2/3} \tag{7b}$$

Eqs. (7*a*) and (7*b*) can be substituted into Eq. (6), and using geometry it is found that the parabolic shape of the deflected VBS's actual coordinates can be written as

$$x = \frac{y^2}{2r_0} \tag{8}$$

where r_0 = the radius of curvature at the base of the parabola given as

$$r_0 = \frac{1.34^2}{2(\eta)^{2/3}} \tag{9}$$

Harnett et al. (2011) related the deflected VBS shape in bending to electrical resistance. The total resistance in the VBS bending element, R_{total}, can be found by integrating the resistance per unit length as a function of the local radius of curvature as

$$R_{\text{total}} = \int_0^{y_{\text{end}}} R'[r_{\text{local}}(y)]ds(y) \tag{10}$$

where y_{end} = the coordinate for the end of the resistive strip; R' = the resistance per unit length; r_{local} = the local radius of curvature; and $ds(y)$ = the local arc length. y_{end} can be found analytically by integrating the local arc length as

$$l = \int_0^{y_{\text{end}}} ds(y) = \int_0^{y_{\text{end}}} \sqrt{1 + \left(\frac{y}{r_0}\right)^2}\, dy \tag{11}$$

where l = the length of the VBS bending element. Integration of Eq. (11) yields

$$l = \frac{1}{|2r_0|}\left[r_0^2 \ln\left(\frac{\sqrt{r_0^2 + y_{\text{end}}^2} + y_{\text{end}}}{|r_0|}\right) + y_{\text{end}}\sqrt{r_0^2 + y_{\text{end}}^2}\right] \tag{12}$$

Since l is known and r_0 is given by Eq. (9), y_{end} is calculated with the zero crossing as

$$\left[r_0 \ln\left(\frac{\sqrt{r_0^2 + y_{\text{end}}^2} + y_{\text{end}}}{|r_0|}\right) + y_{\text{end}}\sqrt{r_0^2 + y_{\text{end}}^2}\right] - 2l = 0 \tag{13}$$

In Eq. (10), R' = a function of the radius of curvature and can be estimated empirically (Harnett et al. 2011) as

$$R' = e^{C_{\text{VBS-1}}} r^{C_{\text{VBS-2}}} + \frac{10V_0}{l(5 - V_0)} \tag{14}$$

where r = the radius of curvature; $C_{\text{VBS-1}}$ and $C_{\text{VBS-2}}$ = calibration parameters specific to an individual VBS; and $10V_0/[l(5 - V_0)]$ = the resistance per unit length of the nondeflected VBS found by measuring the resistance of individual nondeflected bending elements, V_0, and dividing by its length, l. r_{local} is found from calculus (Stewart 2008) to be

$$r_{\text{local}}(y) = r_0\left[1 + \left(\frac{y}{r_0}\right)^2\right]^{3/2} \tag{15}$$

and can be calculated for the deflected VBS shape using Eqs. (8) and (9). After calculating R_{total} with Eq. (10), the voltage divider law can be used to calculate the voltage, V, for the fixed 10 kΩ resistor as

$$V = 5\left[\frac{R_{\text{total}}(r_0)}{R_{\text{total}}(r_0) + 10\ \text{k}\Omega}\right] \tag{16}$$

The semitheoretical approach was applied to the VBS element used in testing and to estimate the time-averaged approach velocity versus output voltage relationship shown in Fig. 3. Table 2 compiles the measured inputs and calibrated coefficients used in the analyses. The approach was applied in two stages. First, C_t was adjusted to fit the theoretical potential flow shape of the bending element proposed by Alben et al. (2002, 2004) to the actual VBS shape found in the turbulent flow experiments. Second, the two calibration coefficients, $C_{\text{VBS-1}}$ and $C_{\text{VBS-2}}$, used to empirically estimate resistance per unit length were found by minimizing the sum of square errors between the estimated output voltage and the measured output voltage.

In the first stage of calibration, Eqs. (5) and (9) were substituted into Eq. (8) as

$$x = \left[0.9C_t^{2/3}\left(\frac{\rho w L^3 U^2}{EI}\right)^{1/3}\right]y^2 \tag{17}$$

Photographs of the VBS bending during the experiments [see Figs. 4(a–c)] were digitized to provide the experimental shapes. Figs. 4(d–f) show calibrated results with the digitized, experimental

Table 2. Measured Inputs and Calibration Coefficients in the VBS Bending Analysis

Symbol	Description	Value	Units	Means of acquisition
C_t	Turbulence coefficient	28	Dimensionless	Calibrated
E	Young's modulus of elasticity	2.55	GPa	Constant
f	Width	8	mm	Measured
L	Length of VBS	41.2	mm	Measured
l	Length of resistive strip	36.5	mm	Measured
$C_{\text{VBS-1}}$	Exponent coefficient in R'	20.6	Dimensionless	Calibrated
$C_{\text{VBS-2}}$	Power coefficient in R'	−6.4	Dimensionless	Calibrated
ρ	Fluid density	1	g cm^{-3}	Constant
V_0	Voltage reading taken when the sensor is undeflected in stagnant conditions	3.0	Volts	Measured

shape and the estimated shape for C_t equal to 28. In general, the calibrated shape compares well. The need for imposing C_t due to lack of exact agreement between the theoretical, self-similar shape described using η and the bending shape during experimentation is reflective of the idealized conditions under which η was derived.

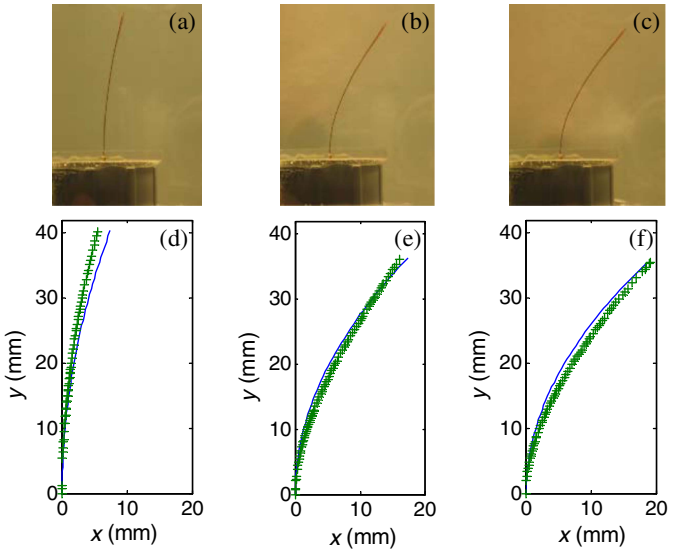

Fig. 4. Photographs of the VBS in bending for U equal to (a) 6.0; (b) 29.4; (c) 35.3 cm s^{-1}; (d–f) digitized VBS shape in bending and predicted VBS shapes (solid line) using Eqs. (6)–(8)

η was formulated in the absence of viscosity via potential flow theory (Alben et al. 2002). Bending in the potential flow case is caused by the pressure difference between the leading and trailing edges of the bending element. In practice, pressure along the trailing edge is set as the freestream pressure since the streamline at the trailing edge cannot be calculated. Alben et al. (2004) suggested η be further scaled to account for the actual wake pressure. In the present case, it is recognized that both viscous effects and the wake pressure difference require C_t. Zhu (2007) recently showed that a bending element in viscous flow experiences increased bending due to viscous effects. In addition, Gosselin et al. (2010) recently highlighted differences in the wake pressure loss that would further increase bending. Further testing using photographs similar to Fig. 4 will be helpful in future research in order to understand how C_t varies under nonidealized cases.

Fig. 5 shows results of the second stage of calibration where the voltage calculated with Eq. (16) is compared to the measured output voltage. Relative VBS voltage is plotted against nondimensional velocity, η, and the time-averaged approach velocity, U. As can be seen, the semitheoretical approach compares well for the calibrated $C_{\text{VBS-1}}$ and $C_{\text{VBS-2}}$. Harnett et al. (2011) found $C_{\text{VBS-1}}$ to range between 6.7 and 7.9 and $C_{\text{VBS-2}}$ to range between −2.6 and −2.7, which is in fairly good agreement with the testing performed here. However, the small differences and the sensitivity of $C_{\text{VBS-1}}$ especially highlights the need to calibrate individual bending sensors prior to application. In further application and practice, the relationship U given V can be solved implicitly using a fairly small data set due to the use of the semitheoretical approach. The authors recommend verification of C_t for specific flow cases (e.g., using an underwater camera in the field); thereafter a minimum of two measurements could be used to parameterize $C_{\text{VBS-1}}$ and $C_{\text{VBS-2}}$ for individual VBS. Additionally, it should be pointed out that once calibrated to the flow configuration, the semitheoretical approach predicts the output voltage well and provides a tool for calibrating other bending type sensors in other fluids.

Turbulence Measurements

Postprocessing of the VBS signal was performed to investigate its ability to provide information about turbulence characteristics of open channel flow over a rough bed. Because the VBS provides only one-dimensional velocity, turbulence measurements of the VBS were compared with the streamwise velocity component measured by the ADV. Testing was compared for the stream-associated hydraulic conditions including hydraulically rough, low relative

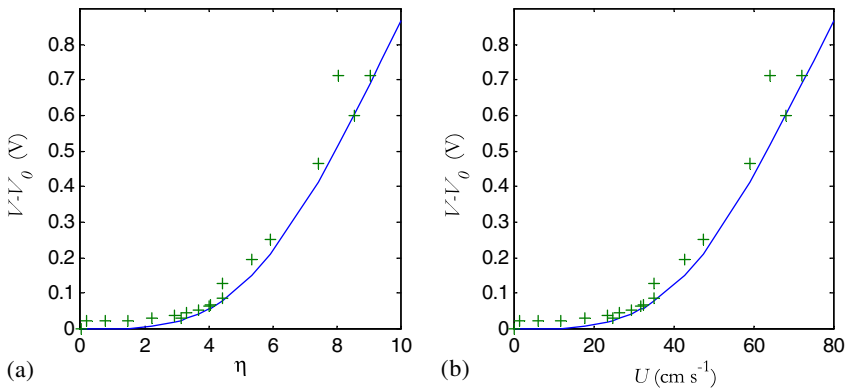

Fig. 5. (a) VBS voltage plotted against nondimensional velocity η; (b) VBS voltage plotted against time-averaged approach velocity

J. Hydraul. Eng. 2013.139:696-706.

submergence of bed particles and moderate Froude number. The turbulent structure of the flow has been well measured and described for these hydraulic conditions using digital particle image velocimetry, large-scale particle image velocimetry, and ADV measurements (Fox et al. 2005; Fox and Patrick 2008; Rodriguez and Garcia 2008; Belcher and Fox 2009; Fox and Belcher 2011). The structure of turbulence for these conditions consists of connected vortex packets that shed from gravel particles and eject away from the bed to form alternating high momentum/low momentum cells termed macroturbulence in the outer region of the flow (Duncan 1970; Adrian et al. 2000; Roy et al. 2004; Hurther et al. 2007; Fox and Belcher 2011). Turbulence for these conditions tends to make two general imprints on the instantaneous streamwise velocity signal including (1) high-frequency fast velocity fluctuations

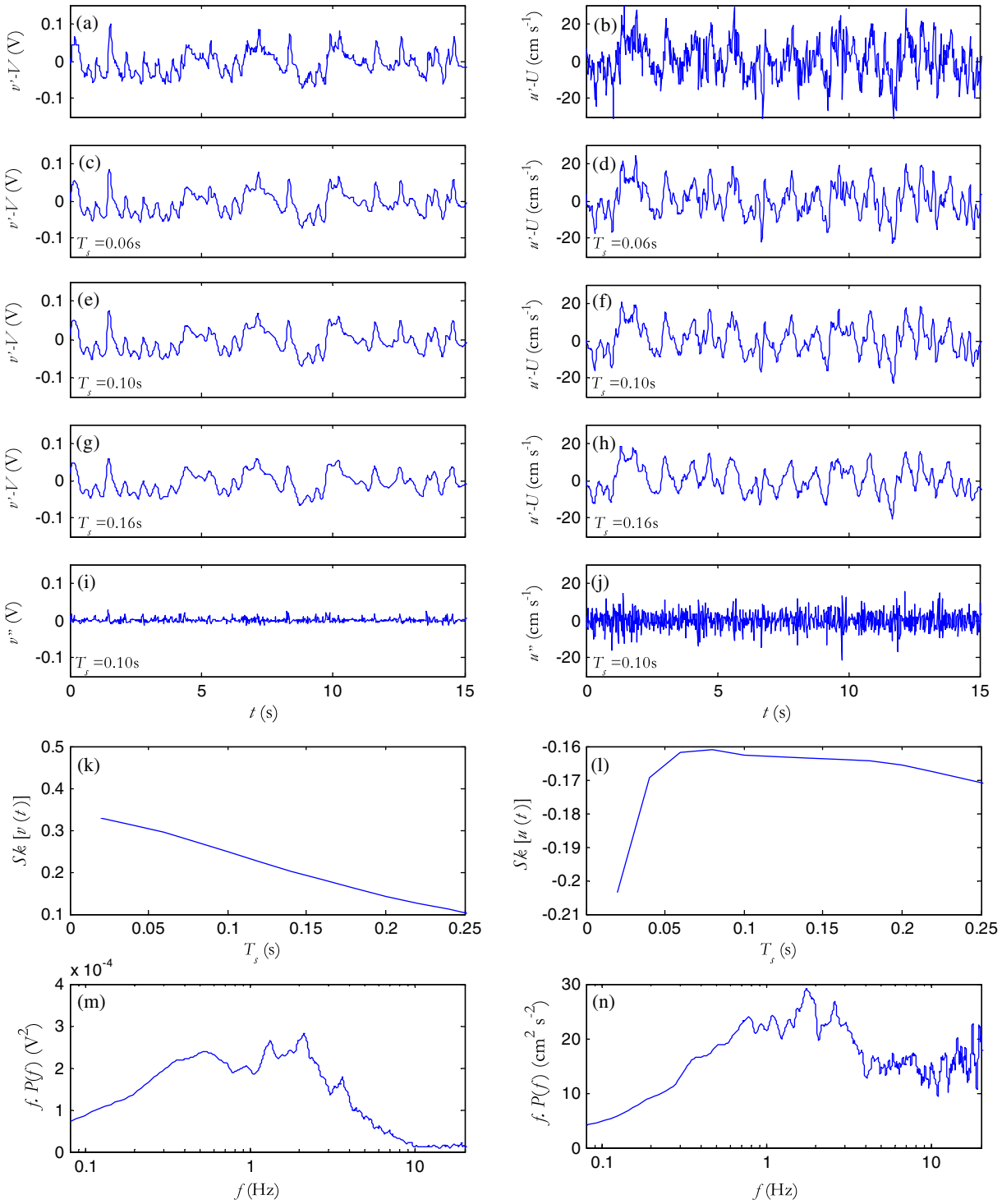

Fig. 6. Time-series analysis for the VBS (left column) and ADV (right column); (a and b) unfiltered time-series data for Test 17; (c–h) results of slow fluctuating component of the triple decomposition theorem for successive moving-average time steps; (i and j) results of the fast fluctuating component of the triple decomposition theorem for T_s equal to 0.10 s; (k and l) skew curves for VBS voltage and ADV streamwise velocity as a function of T_s; (m and n) spectral plots of the VBS voltage and ADV streamwise velocity in variance preserving form

J. Hydraul. Eng. 2013.139:696-706.

associated with vortices shed at the bed, and (2) low-frequency slower velocity fluctuations associated with macroturbulence.

Scale decomposition and spectral analysis were used to isolate the imprint of shed vortices and macrotubulence upon the instantaneous velocity time series of VBS and ADV data. Scale decomposition via the triple decomposition theorem (Hussain and Reynolds 1972) was employed to separate the velocity signal into components having different scales of time as

$$u(t) = U + u'(t) + u''(t) \tag{18}$$

where u = the instantaneous signal; U = the temporal mean; u' = the low-frequency, large-scale signal used to isolate macroturbulence; and u'' = the remaining high-frequency, small-scale signal associated with shedding. u' was isolated using the moving average over a time step T_s as

$$U + u'(t) = \frac{1}{T_s}\int_{t-\frac{T_s}{2}}^{t+\frac{T_s}{2}} u'(t')dt' \tag{19}$$

Selection of an appropriate value for T_s where the small-scale signal is removed was performed using visual inspection of smoothed time series as well as the skew of u' for varying values of T_s (Fox et al. 2005; Lacey and Roy 2008; Fox and Patrick 2008). The skew, S_k, was calculated as

$$S_k = \frac{\frac{1}{n}\sum_{i=1}^{n}(u_i - U)^3}{\left[\sqrt{\frac{1}{n}\sum_{i=1}^{n}(u_i - U)^2}\right]^3} \tag{20}$$

Spectral analysis of the time-series signal was performed to quantify the energy frequency scales of the turbulence. The spectrum was estimated using the discrete Fourier transform of u and v with the fast Fourier transform method as

$$X(f) = \sum_{j=1}^{n} Z_j e^{(-2\pi i)(j-1)(fn/25-1)/n} \tag{21}$$

where the input variable Z = the v or u time series. When plotted in variance-preserving form, broad peaks in the spectral energy density correspond to the frequency of an energetic mean or dominant eddy passing the velocity sensor (Boppe and Neu 1995; Venditti and Bennett 2000).

Results of scale decomposition and spectral analysis for the VBS and the ADV signals are shown in Fig. 6. Figs. 6(a and b) show unfiltered VBS (left column) and ADV (right column) 15 s segments of the total data sets. It should be pointed out that the VBS and ADV data sets in the left and right columns are not synchronized to show the matching of individual, instantaneous fluctuations but rather show how fluctuations compare in general. The VBS is in general smoother than the ADV data showing less-fast fluctuations associated with small-scale turbulent processes. The VBS time series shows low-frequency velocity fluctuations that agree with the ADV time series and are indicative of passing macroturbulent cells. Results of the triple decomposition analysis agree with the time-series observations. u' under varying T_s [Figs. 6(c–h)] shows the low-frequency, large-scale signal associated with macroturbulence for both the VBS and ADV results. u'' variation [Figs. 6(i and j)] is much smaller in magnitude for the VBS as compared to the ADV indicating the lack of ability to capture the high-frequency, small-scale turbulent signal associated with shedding for these hydraulic conditions. Figs. 6(k and l) show results of the skew analysis. Skew of u' for varying values of T_s has shown the ability to aid in the identification of T_s where fast fluctuations within the velocity signal are effectively removed, which occurs when the skew plot displays significant changes (Fox et al. 2005; Lacey and Roy 2008; Fox and Patrick 2008). The ADV skew plot reaches a maximum around T_s 0.8 s, which corresponds to the visual interpretation from the moving-average time plot with T_s of 0.10 s, which appears to eliminate the fast fluctuating component of velocity. The VBS is unable to measure the small-scale fast fluctuating component of velocity, and the skew plot lacks indicators for the threshold T_s. The spectra of the VBS and the ADV show a broad peak on the order of 2 Hz, which indicates the frequency of an energetic mean or dominant eddy size passing the sensor (Boppe and Neu 1995; Venditti and Bennett 2000). In this case, the 2 Hz peak is indicative of the passing of macrotubulence seen visually in the time-series results. The ADV spectrum shows energy at frequencies above 10 Hz associated with the fast fluctuating components of velocity indicative of small-scale turbulence. The inability of the VBS to measure the fast fluctuating component of velocity results in the lack of energy above 10 Hz. The VBS spectrum agrees with the conclusions drawn from the moving average and skew analysis in that the VBS is unable to measure small-scale turbulence but has the capability to capture the low-frequency macroturblence present in the flow.

A final analysis was performed to look at the turbulent intensity of the flow as an overall measure of the fluids turbulent nature. Turbulence intensity is calculated as

$$I_i = \frac{1}{Z}\left[\frac{1}{n}\sum_{i=1}^{n}(z_i - Z)^2\right]^{0.5} \tag{22}$$

where i = turbulent intensity calculated for the VBS or ADV; and Z = a placeholder for V or U. The nondimensional relative turbulent intensity [Eq. (22)] is used for comparison between the ADV and VBS because it does not depend strongly on calibration parameters of the velocimeter (Nezu and Nakagawa 1993, p. 59). It is realized that the nonlinearity of the velocity voltage relationship will cause an error in the relative turbulent intensity predicted by the VBS. It is assumed that the voltage velocity relationship near the time-averaged velocity being measured is approximately linear. Fig. 7 provides a scatter plot of turbulence intensity calculated for the VBS and ADV at the same location in the flow. As can be seen, measurements of turbulent intensity with the VBS are approximately 12% of that recorded with the ADV. The discrepancy between the VBS and ADV measurements reflects the inability of the VBS to measure the smaller-scale turbulence for these conditions. At the same time, the correlation between $I_{x,\mathrm{VBS}}$ and $I_{x,\mathrm{ADV}}$

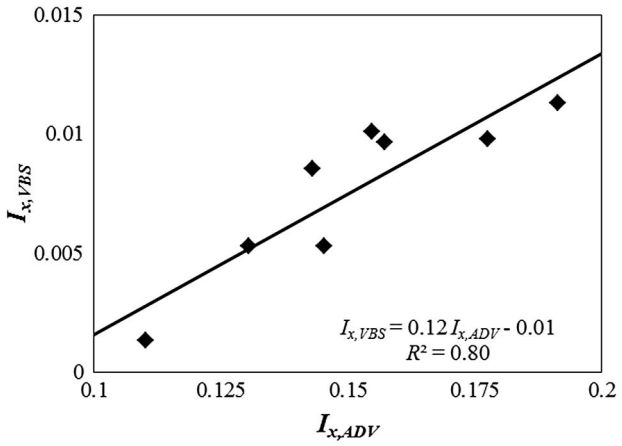

Fig. 7. Turbulent intensity comparison for VBS voltage and ADV streamwise velocity

J. Hydraul. Eng. 2013.139:696-706.

is promising and reflects the ability of the VBS to capture the underlying structure of the turbulent flow. The linear fit between $I_{x,\mathrm{VBS}}$ and $I_{x,\mathrm{ADV}}$ suggests that the VBS could be used as a proxy for more detailed turbulent measurements and could provide some indication of the overall turbulent nature of the flow.

Conclusions

The mechanical, electrical, and wireless transmission characteristics of the newly developed inexpensive wireless VBSs were presented here. Thereafter, the capability of the VBS to measure (1) streamwise time-averaged approach velocity, and (2) turbulence in a hydraulically rough open channel flow was tested.

The VBS tests showed that the sensors were capable of measuring the streamwise time-averaged approach velocity. Only small voltage differences existed for velocities below a threshold velocity where deflections were small; however, above the threshold velocity an appreciable voltage output is measured that will allow field application. A semitheoretical calibration approach based on fluid drag and elastic member bending was developed to estimate the streamwise time-averaged approach velocity from the VBS voltage output. The shape parameter of the semitheoretical approach agreed well with measurements of the deflected VBS shape during experiments after correcting for viscous flow and wake pressure effects. Further, experimental results agreed well with the semitheoretical approach after calibrating empirical parameters for resistance per unit length of the VBS. In further application and practice, the relationship between velocity and voltage for individual VBS can be solved implicitly using a fairly small data set due to the use of the semitheoretical approach.

The ability of the VBS to measure turbulence of hydraulically rough bed flow were analyzed using eddy decomposition via the triple decomposition theorem, spectral analysis, and turbulence statistics. The results show that the VBS could not resolve small-scale turbulence associated with vortex shedding off gravel particles at the streambed but were capable of measuring low-frequency macroturbulence. The streamwise turbulent intensity measured by the VBS was found to be approximately linear and 12% of that recorded with the ADV for the tested flow conditions. The turbulence results suggest that the VBS can be helpful as a proxy for more detailed turbulent measurements and could provide some indication of the overall turbulent nature of the flow in the streams.

Advancements in technology have made the development of these sensors possible and, when integrated into environmental stream monitoring efforts, will provide a wealth of velocity and turbulence data for researchers. The newly developed inexpensive wireless VBS capable of measuring time-averaged velocity and turbulence will be a valuable tool for highly sensed stream monitoring efforts where multiple velocity measurements are necessary to span the spatial scales relevant to environmental parameters of interest. Fig. 8 conceptualizes field deployment of the VBS for measuring turbulence and time-averaged flow conditions in a stream. The wireless capabilities of the sensors will enable faster installation of hydraulic measurement networks. The low cost of the sensors makes deployment possible across spatial scales that have previously been cost prohibitive. Low cost and wireless capabilities provide researchers the ability to monitor remote and dangerous environments that would be difficult to monitor with other sensors. And, the use of inexpensive sensors is especially attractive because of the potential for losing the sensors during high flow events.

Although field deployment of sensor networks is promising, the potential limitations of the VBS should be considered during field deployment. VBS fatigue or creep—the irreversible increase in the sensor dimensions due to temperature or loading conditions—is a potential limitation in future field deployment. Assessment of creep for the polyimide material used in the VBS has been extensive due to the current use of polyimide in electronics for flexible circuit boards. In the VBS experiments, temperature conditions were low (room temperature), and a maximum loading on the sensors equal to 12.5 MPa was reached. Using the elongation ratio as a measure of creep, these temperature and loading conditions would provide an elongation ratio less than 0.5% for the 200 μm polyimide VBS far below the proportional limit (see Figs. 5, 9, and 10 in Chang et al. 2008 for polyimide materials), which is negligible

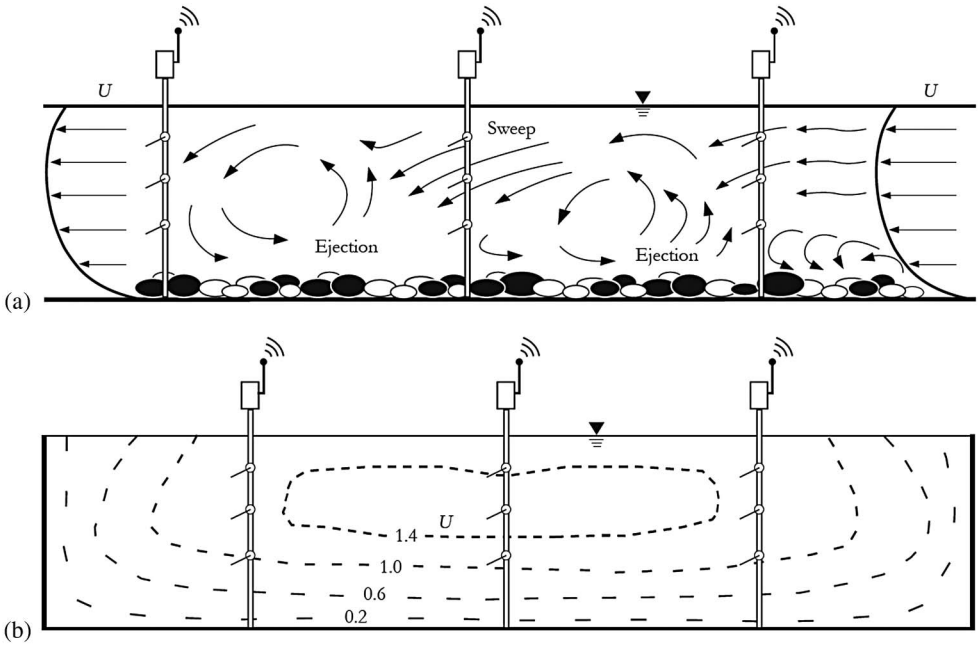

Fig. 8. (a) Depiction of VBS measuring macroturbulence in a stream; (b) VBS measuring time-averaged flow to construct U isovels in cm s^{-1} for a cross section

J. Hydraul. Eng. 2013.139:696-706.

creep. During field deployment, water temperature of streams is not expected to induce creep of the polyimide VBS. However, extreme loading via high-magnitude hydrologic events would have the potential to cause creep of the polyimide sensors. Further, solid debris (e.g., large woody debris) transported during hydrologic events could potentially destroy the bend sensors. The VBS sensors also have limitations at the upper end of their range (i.e., high velocities) and should include an appropriate U_{max} setting. This was also pointed out in bend sensor research by Harnett et al. (2011). The resolution of the bend sensor decreases asymptotically to zero as the sensor element aligns with the flow. Resolution is given by $\Delta V/\Delta U$, where ΔU is the change in flow rate, and ΔV is the change in output voltage. Reduced sensitivity occurs at U_{max} because the sensor aligns nearly completely with the flow, its shape changes very little at these high velocities, and its output voltage is a function of the sensor shape. An appropriate U_{max} setting will be particularly important in field deployment where hydrologic conditions can be highly variable. U_{max} can be increased if a thicker polyimide VBS is used, and the semitheoretical model presented in this paper can be used as a predictive method for U. To this end, field deployment might benefit from numerous VBS with varying thickness to accurately capture a wide range of hydrologic events. Like many field deployable sensors, the VBS is subject to fouling by organic debris such as leaves or algae if deployed for long periods of time, and the VBS should be properly installed in-stream to measure streamwise velocity. Routine maintenance of field deployed VBS should be included in future field methods.

Acknowledgments

The authors would like to thank Alex Thompson, Bill Ford, Ben Zinninger, Thomas Lawrence, and Cory Franklin for building the VBS and for their help with data collection. They thank Prof. Sean Bailey, Mechanical Engineering at the University of Kentucky and Mark Miller for use of, and assistance with, the water tunnel. The authors acknowledge support from National Science Foundation Award No. 0918856. They thank two anonymous reviewers and the associate editor, whose comments helped improve the quality of this paper.

Notation

The following symbols are used in this paper:

B = log-law constant of integration for hydraulically rough flows;
C_t = turbulence coefficient;
C_{VBS-1} = exponential coefficient in empirical resistance;
C_{VBS-2} = power coefficient in empirical resistance;
dH/dx = hydraulic gradient;
$ds(y)$ = local arc length;
d_{84} = diameter of bed particles for which 84% are finer;
E = modulus of elasticity;
F = Froude number;
f = spectral frequency;
g = gravitational constant;
H = mean flow depth;
I = beam moment of inertia;
$I_{x,ADV}$ = turbulence intensity measure with the ADV;
$I_{x,VBS}$ = turbulence intensity measure with the VBS;
j = index in fast Fourier transform;
k = index in fast Fourier transform;
k_s = bed roughness height;
k_s^+ = roughness Reynolds number;
L = length of the VBS;
l = length of the VBS resistive element;
n = number of data points used during the spectral analysis;
$P(f)$ = spectrum of time series;
R = channel Reynolds number;
R_{total} = total resistance of the VBS bending element;
R' = resistance per unit length;
r_{local} = local radius of curvature;
r_0 = radius of curvature at the base of the deflected VBS;
S = bed slope;
S_k = skew, third statistical moment;
T_s = moving-average time step;
U = streamwise time-averaged approach velocity;
U_{bulk} = bulk velocity;
U_* = shear or friction velocity;
u = instantaneous velocity;
u' = low-frequency velocity fluctuations associated with macroturbulence;
u'' = high-frequency velocity fluctuations associated with vortex shedding;
V = time-averaged voltage output from the VBS;
V_0 = voltage reading for undeflected, stagnant conditions;
v = instantaneous voltage output from the VBS;
w = width of the VBS;
X = scaled streamwise coordinate of the VBS;
x = actual streamwise coordinate of the VBS;
Y = scaled lateral coordinate of the VBS;
y = actual lateral coordinate of the VBS;
y_{end} = y-coordinate for the end of the resistive strip;
β = pressure gradient parameter;
η = dimensionless freestream speed;
κ = von Karman constant;
ν = kinematic viscosity of the fluid;
Π = Cole's wake strength;
ρ = fluid density; and
τ_0 = bed shear stress.

References

Adrian, R. J., Meinhart, C. D., and Tomkins, C. D. (2000). "Vortex organization in the outer region of the turbulent boundary layer." *J. Fluid Mech.*, 422, 1–54.
Alben, S., Shelley, M., and Zhang, J. (2002). "Drag reduction through self-similar bending of a flexible body." *Nature*, 420(6915), 479–481.
Alben, S., Shelley, M., and Zhang, J. (2004). "How flexibility induces streamlining in a two dimensional flow." *Phys. Fluids*, 16(5), 1694–1713.
Belcher, B., and Fox, J. (2009). "Discussion of 'Laboratory measurements of 3-D flow patterns and turbulence in straight open channel with rough bed' by J. F. Rodriguez and M. H. Garcia." *J. Hydraul. Res.*, 47(5), 685–688.
Belcher, B. J., and Fox, J. F. (2011). "Outer scaling for open channel flow over a gravel bed." *J. Eng. Mech.*, 137(1), 40–46.
Boppe, R. S., and Neu, W. L. (1995). "Quasi-coherent structures in the marine atmospheric surface layer." *J. Geophys. Res.*, 100(C10), 20635–20648.
Buffin-Belanger, T., and Roy, A. G. (2005). "1min in the life of a river: Selecting the optimal record length for the measurement of turbulence in fluvial boundary layers." *Geomorphol.*, 68(1–2), 77–94.
Chang, W. Y., Fang, T. H., and Lin, Y. C. (2008). "Physical characteristics of polyimide films for flexible sensors." *Appl. Phys. A*, 92(3), 693–701.
Dancey, C. L. (1990). "Measurements of second order turbulence statistics in an axial flow compressor via 3-component LDA." *AIAA, SAE, ASME, and ASEE, 26th Joint Propulsion Conf.*, Orlando, FL.
Duncan, W. J. (1970). *Mechanics of fluids*. Elsevier, New York.

J. Hydraul. Eng. 2013.139:696-706.

Fox, J. F., and Belcher, B. J. (2011). "Comparison of macroturbulence measured using decomposition of PIV, ADV and LSPIV data." *J. Hydraul. Res.*, 49(1), 122–126.

Fox, J. F., Papanicolaou, A. N., and Kjos, L. (2005). "Eddy taxonomy methodology around a submerged barb obstacle within a fixed rough bed." *J. Eng. Mech.*, 131(10), 1082–1101.

Fox, J. F., and Patrick, A. (2008). "Large-scale eddies measured with large scale particle image velocimetry." *Flow Meas. Instrum.*, 19(5), 283–291.

Gosselin, F., Langre, E., and Machado-Almeida, B. A. (2010). "Drag reduction of flexible plates by reconfiguration." *J. Fluid Mech.*, 650, 319–341.

Harnett, C. K., Schueler, M. T., Blumenthal, N. R., Hopf, K. L., Fox, J. F., and Pulugurtha, S. (2011). "Calibration and field deployment of low-cost fluid flow-rate sensors using a wireless network." *IEEE Trans. Instrum. Meas.*, 60(2), 633–641.

Hart, J. K., and Martinez, K. (2006). "Environmental sensor networks: A revolution in the earth system science?" *Earth-Sci. Rev.*, 78(3–4), 177–191.

Hauer, F. R., and Lamberti, G. A. (2006). *Methods in stream ecology*, Academic Press, Amsterdam.

Horsburgh, J. S., Jones, A. S., Stevens, D. K., Tarboton, D. G., and Mesner, N. O. (2010). "A sensor network for high frequency estimation of water quality constituent fluxes using surrogates." *Environ. Modell. Software*, 25(9), 1031–1044.

Hurther, D., Lemmin, U., and Terray, E. A. (2007). "Turbulent transport in the outer region of rough-wall open-channel flows: The contribution of large coherent shear stress structures (LC3S)." *J. Fluid Mech.*, 574, 465–493.

Hussain, A. K., and Reynolds, W. (1972). "The mechanics of an organized wave in turbulent shear flow." *J. Eng. Mech.*, 54(2), 241–261.

Kirkgoz, M. S. (1989). "Turbulent velocity profiles for smooth and rough open channel flow." *J. Hydraul. Eng.*, 115(11), 1543–1561.

Kwan, T. F. (1988). "A study of abutment scour." *Rep. No. 451*, Dept. of Civil Engineering, Univ. of Auckland, Auckland, New Zealand.

Lacey, R. W. J., and Roy, A. G. (2008). "Fine-scale characterization of the turbulent shear layer of an instream pebble cluster." *J. Hydraul. Eng.*, 134(7), 925–936.

Maier, H. R., Jain, A., Dand, G. C., and Sudheer, K. P. (2010). "Methods used for the development of neural networks for the prediction of water resource variables in river systems: Current status and future directions." *Environ. Modell. Software*, 25(8), 891–909.

Nezu, I. (2005). "Open-channel flow turbulence and its research prospect in the 21st century." *J. Hydraul. Eng.*, 131(4), 229–246.

Nezu, I., Kadota, A., and Nakagawa, H. (1994). "Turbulent structures in accelerating and decelerating open-channel flows with laser Doppler anemometer." *9th Cong. of APD-IAHR*, Singapore, Vol. 1, 413–420.

Nezu, I., and Nakagawa, H. (1993). *Turbulence in open channel flows*, Balkema, Rotterdam.

Onitsuka, K., Akayama, J., and Matsuoka, S. (2009). "Prediction of velocity profiles and Reynolds stress distributions in turbulent open-channel flows with adverse pressure gradient." *J. Hydraul. Res.*, 47(1), 58–65.

Rehmel, M. (2007). "Application of acoustic doppler velocimeters for streamflow measurements." *J. Hydraul. Eng.*, 133(12), 1433–1438.

Rodriguez, J. F., and Garcia, M. H. (2008). "Laboratory measurements of 3-D flow patterns and turbulence in straight open channel with rough bed." *J. Hydraul. Res.*, 46(4), 454–465.

Roy, A. G., Buffin-Bélanger, T., Lamarre, H., and Kirkbride, A. D. (2004). "Size, shape and dynamics of large-scale turbulent flow structures in a gravel-bed river." *J. Fluid Mech.*, 500, 1–27.

Rundel, P. W., Graham, E. A., Allen, M. F., Fisher, J. C., and Harmon, T. C. (2009). "Environmental sensor networks in ecological research." *New Phytologist*, 182(3), 589–607.

Singh, A., Porté-Agel, F., and Foufoula-Georgiou, E. (2010). "On the influence of gravel bed dynamics on velocity power spectra." *Water Resour. Res.*, 46(4), W04509.

Song, T., and Chiew, Y. M. (2001). "Turbulence measurement in nonuniform open-channel flow using acoustic Doppler velocimeter (ADV)." *J. Eng. Mech.*, 127(3), 219–232.

Song, T., and Graf, W. H. (1994). "Non-uniform open-channel flow over a rough bed." *J. Hyrosci. Hydraul. Eng.*, 12(1), 1–25.

Stewart, J. (2008). *Calculus early transcendentals*, 6th Ed., Cengage Learning, Stamford, CT.

Venditti, J. G., and Bennett, S. J. (2000). "Spectral analysis of turbulent flow and suspended sediment transport over dunes." *J. Geophys. Res.*, 105(C9), 22035–22047.

Vivoni, E. R., and Camilli, R. (2003). "Real-time streaming of environmental field data." *Comput. Geosci.*, 29(4), 457–468.

Wang, N., Zhang, N., and Wang, M. (2006). "Wireless sensors in agriculture and food industry: Recent development and future perspective." *Comput. Electron. Agric.*, 50(1), 1–14.

Yick, J., Mukherjee, B., and Ghosal, D. (2008). "Wireless sensor network survey." *Comput. Netw.*, 52(12), 2292–2330.

Zhu, H. (2007). "Viscous flow past a flexible fibre tethered at its centre point: Vortex shedding." *J. Fluid Mech.*, 587, 217–234.

J. Hydraul. Eng. 2013.139:696-706.